AIAA-2002-2169

Finite Element Based Hydrodynamic Sheath Model

Subrata Roy and B.P. Pandey
Computational Plasma Dynamics Laboratory
Kettering University
Flint, MI 48504

33rd Plasmadynamics and Lasers Conference
20-23 May 2002
Maui, Hawaii

AIAA-2002-2169

Finite Element Based Hydrodynamic Sheath Model

Subrata Roy* **and B. P. Pandey§**

Computational Plasma Dynamics Laboratory
Kettering University, Flint, MI 48504

In the present work, a finite element discretized one-dimensional formulation of plasma–sheath dynamics, using multi-fluid equations for a partially ionized plasma, is given. Based on the experimental data for multiple ionization of xenon gas, a third order polynomial has been used as a fit to describe ionization processes. Such a polynomial has been used to self-consistently calculate the rate of ionization in the plasma dynamic equations. The electron and ion number densities decrease in the plasma-sheath region as expected. The neutral number density decreases in the bulk plasma region and increases in the sheath region pointing to the dominant role of recombination near the wall. The ion velocity, sheath potential and electron temperature profiles exhibit the expected behavior.

INTRODUCTION

Sheath formation at the plasma-boundary interface separating the quasi-neutral plasma is ubiquitous in a bounded plasma. The physics governing the formation of the boundary layer between the wall and the plasma have been studied for past many decades and are yet to be fully understood. The interest in the subject has been revived recently due to its wide ranging applications in plasma processing; in the ion cyclotron heating; in electric propulsion devices; in fusion plasmas; in high-speed air vehicles. In the electric propulsion devices, built up of sheath potential and its stability may severely affect the thruster efficiency (Morozov and Savelyev[1]). The interaction between the plasma and the limiter, divertor, in a magnetically confined fusion plasma such as tokamak is important in connection to the effect of plasma on the surface and sputtering from the wall to the plasma. Accurate sheath modeling is of considerable interest to the effective design of ionized flow in high-speed air vehicles. Considerable reduction in the aerodynamic drag via plasma or high temperature gas injection from the stagnation region has been reported in weakly ionized gas (Shang et al[2]). In high-speed air vehicles, the interaction of the near-field flow around a supersonic and hypersonic vehicle and an applied magnetic field acting on the ions produced at the bow shock wave can actually produce beneficial effects on drag and heat transfer. These effects can be further controlled by the existence of plasma sheath near the leading surface of the air vehicle. Present status of the space propulsion and hypersonic flow research reflects a dearth of consistent numerical models to understand the effect of near wall plasma interaction with a magnetic field. The anomalies are due to the choice of Bohm's criterion as the boundary condition for both plasma and sheath using a non-consistent model. This paper describes a

* Assistant Professor, Department of Mechanical Engineering, E-mail: sroy@kettering.edu, Associate Fellow, AIAA.
§ Post Doctoral Research Associate, Department of Mechanical Engineering, E-mail: bpandey@kettering.edu, Member, AIAA.

theoretical basis for electrode voltage sheath modeling for such applications.

The build-up of near wall potential due to different mobility of the constituents in an ionized gas is as old a problem as the discovery of plasma itself (Langmuir and Tonks[3]). The specific feature of the plasma sheath near an electrode is the formation of charged boundary layer due to the difference in mobility among different plasma particles viz. electrons and ions in a two component, electron-ion plasma. Since electron mobility is much higher than the ion mobility, the plasma boundary becomes negatively charged leaving behind a positively charged column near the electrode. The resultant potential gradient tends to slow the incoming (to the boundary wall) electrons and accelerate the ions until a steady state is reached, with equal ion and electron fluxes. A stationary sheath exists only if the ion flow velocity satisfies the Bohm criteria at the plasma-sheath boundary i.e plasma drift speed must exceed the ambipolar ion sound speed (Bohm velocity). Though the particle mobility depends upon many factors e.g. electromagnetic field, the principal factor in sheath plasma is the induced dc sheath potential which equates all fluxes, preserving in the process the quasi-neutrality of the bulk plasma.

Thus, a sheath consists of a presheath which is of the order of mean free path of plasma-neutral interaction and where plasma maintains a space-charge neutrality and a Debye-sheath, which is of the order of Debye length λ_D and where a large potential drop occurs. The ions are accelerated in the pre-sheath region so that they enter the sheath region with the minimum energy required for a stable sheath. When one looks at the whole profile of the sheath potential starting at the presheath region (where the approximate charge neutrality holds) up to the Debye sheath region (where the charge neutrality is violated), one sees that the condition in the presheath-Debye sheath transition region depends on various parameters such as the ion flow velocity, the plasma temperature, the neutral density and so on.

Near the sheath region, elastic and inelastic collisions between ions and neutrals may play an important role on the sheath dynamics. One dimensional analytical and numerical analysis of Valentini[4-5] suggest that in a collisional plasma, not only the thickness of the sheath is substantially larger than the Debye length λ_D but also, plasma drift velocity can be smaller than the Bohm velocity. Moreover, since the ratio of characteristic ambipolar ion drift speed to Bohm speed $V_c / V_B = \sqrt{n_i / n_e}$ is greater than one, the electric field determines the charged boundary layer formation in a narrower interval of the ion drift speed than described by the Bohm criteria. Furthermore, V_c is a function of space and thus we see that the general criteria for sheath formation become much more complicated than in the classical Bohm case when V_B is constant provided electron temperature is constant. In fact no lower bound exists on the ion drift velocity in the collisional plasma and Debye length can be of the same order as the ion-neutral collisional mean free path, λ_{mfp} (Valentini[5]). Clearly, Bohm criterion is only sufficient but not a necessary condition for sheath formation.

Thus, it is worth asking how various parameters such as the interaction between the neutral and the plasma affect the formation of the sheath and how does, in the process, the ion acceleration in the channel gets affected. The electron-neutral and ion-neutral collisions play key role in the momentum and energy transfer in a partially ionized plasma and their role on sheath formation is not well understood. On physical ground we shall anticipate that the ion collision in the sheath may reduce the ion impact energy to the wall. Consequently, ion dynamics must encompass the entire range of collisionality. The sheath formation in low-pressure discharge is developed numerically by means of a three-fluid model for compressible media.

The length scale disparity between the bulk plasma and the bounding sheath causes considerable numerical difficulties. The literature on the plasma-sheath modeling suggests that sheath and the plasma region can be modeled separately and treat sheath as a boundary condition to the bulk plasma solution (e.g., Sternberg and Godyak[6-7]). However, for a time dependent sheath, it is not clear how to match properly the sheath to the bulk plasma (Nitschke and Graves[8]). Therefore, a combined plasma-sheath model development is appropriate. In this work, we present a formulation of a combined plasma-sheath model for a partially ionized plasma that includes the effect of ionization and recombination on the plasma dynamics in the presence of neutrals and isothermal ions.

The numerical simulation is based on two-momentum, single-temperature, three-fluid flow equations. We have utilized one-dimensional (1D) sub-grid embedded (SGM) finite elements of Roy and Baker[9-10] for convergence and stability of the steady state solution. Furthermore, without the participation of neutrals, the effect of ionization and recombination cannot be studied satisfactorily. Therefore, we have included the neutral continuity equation in our model with a given, fixed uniform neutral velocity. For estimating the neutral-ion cross-section and collision frequencies, we have assumed that the neutral gas is an inert gas, namely, Xenon. We leave the effect of the secondary emission from the present formulation.

NOMENCLATURE

S_{ioniz} = ionization source
S_{recomb} = recombination source
e = elementary charge, 1.6×10^{-19} C
E_i = Ionization Potential
E = Electric Field, V/m
L = Differential operator
m_i = mass of ion,
m_e = mass of electron, 9.1×10^{-31} kg
n = number density, /m^3
P = pressure, J/m^3
R = solution residual
T = temperature, eV
t = time, s
u, **U** = state variable
V = flow velocity, m/s
α = recombination coefficient
ε_0 = vaccum permeability, F/m
ϕ = plasma voltage, V
Ω = solution domain
ν = collision frequency, 1/s
σ = cross section, m^2
ϑ = numerical implicitness

Subscripts

B = Bohm
e = electron
i = ion
n = neutral
t, th = thermal velocity, m/s
α = electron, ion
0 = neutral
+ = singly ionized
++ = doubly ionized

MODEL DESCRIPTION

In partially ionized plasma, several important elastic and inelastic processes can take place simultaneously. Elastic collision involves only exchange of momentum and energy between colliding particles whereas inelastic processes such as ionization, recombination, charge-exchange collision, secondary emission, sputtering etc. can be responsible for redistributing the number density, momentum and energy of the particles. However, we shall note that not all processes are equally probable. For example, momentum exchange due to electron-electron and ion-ion collisions will not be important in comparison with the electron-ion momentum exchange, as the relative drift between similar particles is small in comparison with the drift between electrons and ions. The collisions between electron-neutral, electron-ion, and ion-neutral play an important role. The plasma-neutral collision usually determines the kinetics of the motion. The

electron-neutral collision frequency is given as $\nu_{en} = n_n < \sigma_{en} V_{eth} >$. Assuming typical electron thermal velocity $V_{eth} \sim 10^6$ m s^{-1} (electron temperature of several eV), with neutral atom density $n_n \sim 10^{17}$ m^{-3}, and $\sigma_{en} \approx 27\times10^{-20}$ m^2 for Xe, we see that the electron-neutral collision frequency is $\nu_{en} \sim 10^4$ s^{-1}. The ion-neutral collision frequency ν_{in} is much smaller than electron-neutral collision frequency ν_{en} as $V_{ith} \sim 10^3$ - 10^4 m s^{-1}.

The rate of ion production in a plasma is determined by the ionization frequency. The rate of ionization is given as

$$S_{ioniz} = n_e n_n \left\langle V_{eth} \sigma_i (V_{eth}) \right\rangle = k_i n_e n_n \qquad (1)$$

where σ_i is the total cross section of the process, n_e is the electron number density and, process constant $k_i = <\sigma_i(V_{eth}) V_{eth}>$ where the averaging is done over the velocities of the electrons whose kinetic energy is sufficient for ionization. A general electron temperature dependent empirical formula can be fitted to the ionization process constant $k_i = [k_i^{0+}, k_i^{0++}, k_i^{1++}]$, where 0+, 0++ and 1++ correspond to the neutral to single and double and single to double ionization respectively. We shall use the following generalized process rate that is a sum of all three ionization rates,

$$k_i = (-3.2087\times10^{-5}\ T_e^3 - 0.0022\ T_e^2 + 0.7101\ T_e - 1.76)\times10^{-14} \qquad (2)$$

The above estimate of ionization rate is based on the Maxwellian distribution function. The probability of recombination is

$$S_{recom} = -n_e n_i \left\langle V_{eth} \sigma_{ei}^r (V_{eth}) \right\rangle = -\alpha n_e n_i \qquad (3)$$

where recombination coefficient α can be approximated as (Mitchner and Kruger[11])

$$\alpha = 1.09\times10^{-20}\ n_e\ T_e^{-9/2}\ m^3/s \qquad (4)$$

The cross-section for charge exchange collisions for Xe-Xe^+ is given by (Pullins, Chiu, Levandier and Dressler[12])

$$\sigma\left(Xe\text{-}Xe^+\right) = \left(142.21 - 23.30\ \log_{10}(\Delta V)\right) \times 10^{-20}\ m^2 \qquad (5)$$

For a relative velocity ΔV between 10 and 2×10^3 m/s, the charge exchange cross-section is between 10^{-20} to 10^{-19} m^2. Having delineated the important physical processes in the partially ionized plasma, we now give the basic set of equations that describes the sheath-plasma dynamics under investigation.

The continuity equation for electrons and ions,

$$\frac{\partial n_\alpha}{\partial t} + \frac{\partial (n_\alpha V_\alpha)}{\partial z} = S_{ioniz} - S_{recomb} \qquad (6)$$

Here V_α and n_α are the electron and ion velocities and number densities respectively for $\alpha = e$ and i, with S_{ioniz} and S_{recomb} given by equations (1) and (3). The neutral continuity equation is

$$\frac{\partial n_n}{\partial t} + \frac{\partial (n_n V_n)}{\partial z} = S_{recomb} - k_i^{0+} n_e n_n - k_i^{0++} n_e n_n. \qquad (7)$$

The ion momentum equation is,

$$\frac{\partial V_i}{\partial t} + V_i \frac{\partial V_i}{\partial z} = -\frac{T_i}{m_i n_i}\frac{\partial n_i}{\partial z} + \left(\frac{Ze}{m_i}\right)E - \nu_c V_i + \left(\frac{m_e}{m_i}\right)\nu_{ei}(V_e - V_i) - 0.5\ \nu_{in}(V_i - V_n) + \left(S_{recomb} - S_{ioniz}\right)\frac{V_i}{n_i}. \qquad (8)$$

where the factor 0.5 before ion-neutral collision term in the right hand side comes from reduced mass $m_i m_n/(m_i + m_n) \approx m_i/2$. Here, E is the electric field, and ν_{ei} is the electron-ion collision frequency, ν_c is the ion charge-exchange collision frequency, e is the electron charge and Z is the ionicity. The electron momentum equation is given as,

$$\frac{\partial V_e}{\partial t} + V_e \frac{\partial V_e}{\partial z} = -\frac{1}{m_e n_e}\frac{\partial p_e}{\partial z} - \left(\frac{e}{m_e}\right)E - \nu_{ei}(V_e - V_i) + \left(S_{recomb} - S_{ioniz}\right)\frac{V_e}{n_e}. \qquad (9)$$

The electron energy equation is,

$$\frac{3}{2}\left(\frac{\partial T_e}{\partial t} + V_e \frac{\partial T_e}{\partial z}\right) = -T_e \frac{\partial V_e}{\partial z} + \nu_{ei}\left(V_e - V_i\right)^2 + \left(\frac{S_{recomb} - S_{ioniz}}{n_e}\right)\left(\frac{3}{2}T_e - E_i\right). \qquad (10)$$

Finally, the Poisson's equation for potential is,

$$\varepsilon_0 \nabla^2 \varphi = - e \left(n_i - n_e \right) \qquad (11)$$

In the electron energy equation (10), we have ignored the terms due to electron-neutral energy exchange, as the neutral dynamics have been left out of the present formulation. Furthermore, contribution due to the exchange of random thermal energy has also been ignored and only the dominant contribution due to the exchange of mean flow energy between electrons and ions has been retained.

Before numerically solving above set of equations (6)-(11), we normalize the physical variables. All dependent variables can be normalized using

$$V_B = \sqrt{\frac{2\ T_e}{m_i}}\ ; \quad \nu_{ref} = \sigma_{ref} n_{ref} V_B\ ;\ \phi = \left(\frac{e\ \varphi}{T_e} \right),$$

where $\sigma_{ref} = \sigma_0 \sqrt{\frac{m_i}{m_e}}$, $\sigma_0 \cong 3.6 \times 10^{-20}$ m^2 for Xe.

The fundamental length scale l_0 can be defined in terms of characteristic Bohm velocity V_B and collisional frequency, $l_0 = V_B/\nu_{ref}$. The time scale is $t_0 = \nu_{ref}^{-1}$.

We need to specify proper initial and boundary conditions in order to complete the formulation of the sheath problem. In a combined plasma-sheath model, boundary conditions are used to provide the coupling between plasma and sheath regions (Nitschke and Graves[8]). We impose zero plasma velocity and Dirichlet condition on ion density at the upstream boundary of the simulation box. At the plasma-sheath interface, we ensure that the ion velocity is equal to the modified Bohm velocity (Godyak and Sternberg[7])

$$V_B = \sqrt{\frac{2\ \left(T_e + T_i \right)}{m_i}} \left(1 + \frac{\pi \lambda_D}{2 \lambda_i} \right)^{-1/2} \qquad (12)$$

where $\lambda_D = (\varepsilon_0\ T_e\ / e^2\ n_e\ )^{1/2}$ is the electron Debye length and λ_i is the "effective" ion mean free path which is defined as $V_B/(\nu_{in} + \nu_{ie} + \nu_c)$. The electron density at the wall is homogeneous Dirichlet. We impose the electric field at the plasma-sheath boundary as

$$\left| \frac{d\varphi}{dz} \right|_{z=z_1} = \frac{T_e}{e \lambda_{D1}}, \qquad (13)$$

where λ_{D1} is the electron Debye langth at the sheath-presheath boundary. The wall is maintained at a negative potential. The neutral density is imposed at the inlet and homogeneous Neumann condition is imposed on the remaining boundary. The neutral velocity is assumed to have a uniform value everywhere.

FINITE ELEMENT BASED MODELING

A general formulation for (6)-(11) may be expressed as $L(\mathbf{U})=0$, where $\mathbf{U}=\{n_i, n_e, n_n, V_i, V_e, T_e, \phi\}^T$ and L is a differential operator. The weak statement underlines the development of the range of CFD algorithms. Such an integral statement associated with (6)-(11) is

$$\int_\Omega w L(\mathbf{U}) d\Omega = 0 \qquad (14)$$

where w denotes any admissible test function (Roy[13]). Thereafter, the finite element (FE) spatial semi-discretization of the domain Ω of (6)-(11) employs the mesh $\Omega^h = \cup_{el} \Omega_{el}$ and Ω_{el} is the generic computational domain. Using superscript "h" to denote "spatial discretization," the FE weak statement implementation for (14) defines the approximation as

$$u(x_j) \approx u^h(x_j) = \bigcup_{el} u_{el}(x_j) \text{ and } u_{el}(x_j) = N_k \mathrm{U}_{el}$$

where u is any variable in $\mathbf{U}$ and N is the appropriate basis function that may be represented by Chebyshev, Lagrange or Hermite interpolation polynomials complete to degree k, plus perhaps "bubble functions" (Roy and Baker[10]).

The spatially semi-discrete FE implementation of the *weak statement* WS^h for (14) leads to

$$WS^h = S_e \left(\int_{\Omega_e} N_k L_e(\mathbf{U}) d\tau \right) \qquad (15)$$

S_e symbolizes the "assembly operator" carrying local (element) matrix coefficients into the global arrays. Application of Green-Gauss divergence theorem in equation (15) may yield natural homogenous Neumann boundary conditions and the surface integral that contains the unknown

boundary fluxes wherever Dirichlet (fixed) boundary conditions are enforced.

Independent of the physical dimension of Ω, and for general forms of the flux vectors, the semi-discretized weak statement of (15) always yields an ordinary differential equation (ODE) system:

$$\mathbf{M}\, d\mathbf{U}/dt + \mathbf{R}(\mathbf{U}) = \mathbf{0}, \qquad (16)$$

where $\mathbf{U}(t)$ is the time-dependent finite element nodal vector. The time derivative $d\mathbf{U}/dt$, is generally replaced by using a ϑ-implicit or τ-step Range-Kutta time integration procedure. In (16), $\mathbf{M} = S_e(\mathbf{M}_e)$ is the "mass" matrix associated with element level interpolation, **R** carries the element convection information and the diffusion matrix resulting from genuine (not for Euler) or numerical elemental viscosity effects, and all known data. For steady state, (16) is usually solved using a Newton-Ralphson scheme:

$$\mathbf{U}_{\tau+1}^{i+1} = \mathbf{U}_{\tau+1}^{i} + \Delta\mathbf{U}^{i} = \mathbf{U}_{\tau} + \sum_{p=0}^{i} \mathbf{U}^{p+1}, \text{ where}$$
$$\Delta\mathbf{U}^{i} = -\left[\mathbf{M} + \vartheta\Delta t(\partial\mathbf{R}/\partial\mathbf{U})\right]^{-1}\mathbf{R}(\mathbf{U}) \qquad (17)$$

In (17), ϑ is the implicitness of the numerical algorithm and $0 < \vartheta < 1$. The obvious numerical issues will be associated with calculation of the "jacobian" $\partial\mathbf{R}/\partial\mathbf{U}$ and inversion of the $\mathbf{M}+\vartheta\Delta t(\partial\mathbf{R}/\partial\mathbf{U})$ matrix with sufficient accuracy. Equations (6)-(11) are strongly coupled and the jacobian matrix for this problem becomes very stiff for realistic mass ratio of electron and ion. This results in solution divergence for standard Galerkin finite element approach on a moderate to fine mesh. As a remedy, we utilized a high-order accurate SGM finite element[9-10] method to achieve stable monotone solution on a relatively coarse grid.

The code uses variable time steps till the transient features die down as the iteration converges to a steady state. The solution is declared convergent when the maximum residual for each of the state variable becomes smaller than a chosen convergence criterion of $\in=10^{-4}$. Here, the convergence of a solution vector **U** on node *j* is defined as the norm:

$$\frac{\|\mathbf{U}_j - \mathbf{U}_{j-1}\|}{\|\mathbf{U}_j\|} \le \in \qquad (18)$$

The steady state is declared when the above convergence criteria is met at the first iteration of any timestep.

RESULTS AND DISCUSSION

As has been mentioned above, combined plasma-sheath dynamics is modeled by a 1D geometry. Equation set (6)-(11) is solved using SGM finite element method[9-10] over a computational domain (x=z/L:0,1) where L is the characteristic length of the plasma-sheath region. The mesh consists of 40 equal length 1D quadratic finite elements (i.e., 81 nodes) for all normalized numerical results presented here.

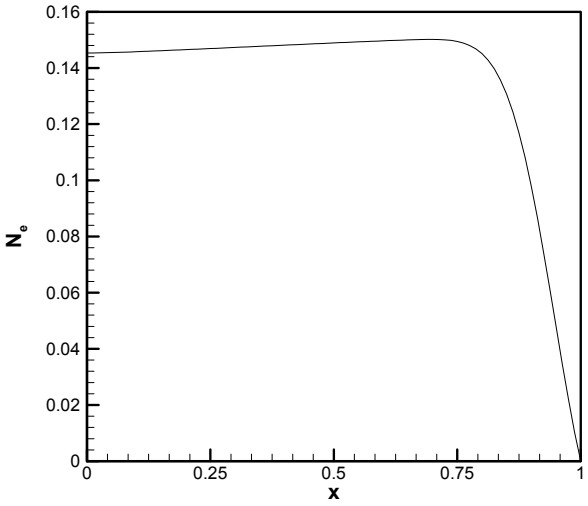

Figure 1. Electron number density profile.

Figure 1 shows the normalized electron number density profile. Evidently, electron number density starts to decrease rapidly near the plasma-sheath boundary and becomes almost zero at the wall. This is expected as due to the build up of a strong negative potential at the wall, electrons will be expelled from the presheath-sheath region and only supra-thermal electrons will be able to overcome the potential barrier and cross over to the wall. The number of supra-thermal electron is always small in any given plasma. The impact of electron-ion recombination near the wall also contributes to the

rapid decline of electron density. Wall acts like a third body and rapid recombination will take place on the surface of the wall. We shall search for the correlation in the neutral number density.

In Fig. 2, normalized ion number density is plotted. The ion number density increases all through the plasma region due to the impact ionization of the electrons and the neutrals. However, in the vicinity of the presheath-sheath boundary, the ion number density starts decreasing. The result can be understood in the following way. Assuming that the sheath has reached a steady state, ion flux will be conserved if the system is in ionization equilibrium. Then, if the ion velocity increases beyond presheath-sheath boundary, then ion number density must decrease, which is reflected in the picture. However, system is not exactly in ionization equilibrium where, recombination and ionization balances each other, as will be seen from the neutral density profile, Fig. 4.

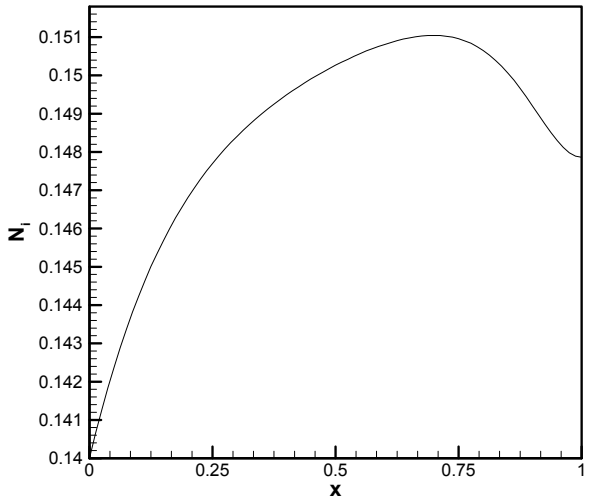

Figure 2. Ion number density profile.

In Fig. 3, ion and electron densities are plotted on the same scale. We see that the plasma remains quasineutral in the bulk plasma and $n_e \approx n_i$. However, there is a considerable departure from quasineutrality near the plasma-sheath boundary. Due to negative potential build up on the wall, electrons are repelled and their number density decreases rapidly whereas, decrease in ion number density is gradual. This is consistent with typical sheath picture near the wall (Chen[14]).

The neutral number density (Fig. 4) shows a rapid decline before recovering near the presheath and recovery continues right to the wall. The decline in the neutral number density in the bulk plasma can be attributed to the dominance of the ionization over recombination. Similarly, increase in the neutral number density near the wall could be attributed to the dominance of recombination over the ionization. The behavior of neutral density profile is well correlated to the electron and ion number density profiles.

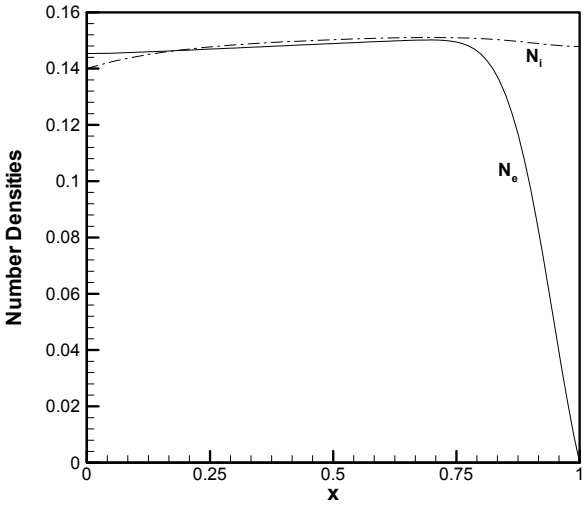

Figure 3. Ion and electron number densities.

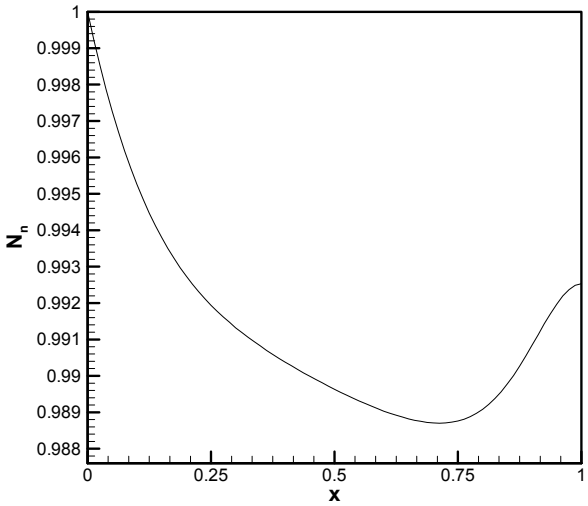

Figure 4. Neutral number density distribution.

The potential and electric field profiles are given in Figs. 5 and 6 respectively. The built up of a large negative potential and corresponding repulsive

electric field near the plasma-wall region is suggested by these figures. The effect of collision has been considered in the form of modified Bohm criteria in equation (12). However, a comparative study of the formation of presheath boundary should be done by switching off the collision terms, to determine any effect of collision on the location of sheath-presheath boundary. Further, the role of neutrals on the boundary layer formation can only be investigated if the proper neutral dynamics is included. Then the presence of the neutral will affect the plasma dynamics through the collisional exchange of momentum and energy.

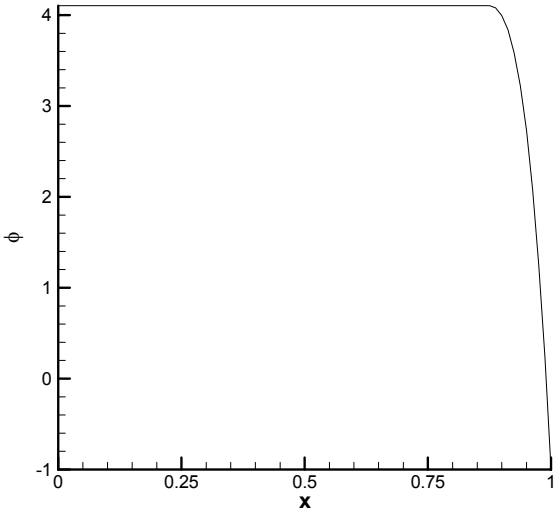

Figure 5. Plasma potential distribution.

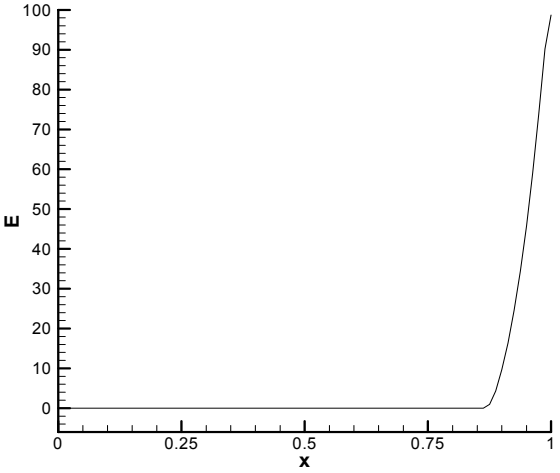

Figure 6. Electric field profile.

In Figure 7, the ions are accelerated toward the negatively charged wall and reach the critical velocity at the presheath-sheath boundary. The ion velocity keeps increasing inside the sheath exceeding Bohm velocity and it finally saturates at the wall. We have noted above that the reduction of ion density inside the sheath can be correlated with the increase in the ion velocity. What happens in the bulk plasma region where also, ion velocity keeps increasing? The plasma is not in equilibrium and thus, above interpretation requires some caution as other processes like charge exchange collision, multiple ionization along with the elastic and inelastic processes are taking place simultaneously. Thus, ion velocity can increase, e.g. at the expense of, neutral velocity. This can be seen clearly if we switch off all other terms in ion momentum equation (8) except ion-neutral collision. We see that constant neutral velocity will give rise to an acceleration ~ 2 (z V_n)$^{1/2}$ which explains the linear increase of the ion velocity.

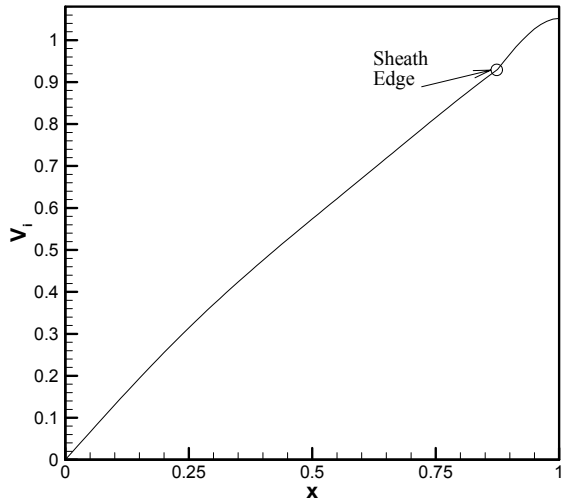

Figure 7. Ion velocity profile.

The electron temperature profile is shown in Figure 8. We note that the spatial evolution of density (Fig. 1) is correlated with the temperature evolution (Fig. 8). In fact this correlation could be anticipated on the physical ground. The number of high energetic electrons will be less than the number of low energy electrons in any given distribution. Therefore, the region of high temperature should reflect a dip in the electron density. The increase in the electron temperature is not rapid. Further, close to the wall, the

temperature profile saturates. Apart from Ohmic heating, electrons also get energy from the inelastic exchange with the ions and the neutrals. The effect of temperature on the sheath is only indirect in the present model and requires further investigation.

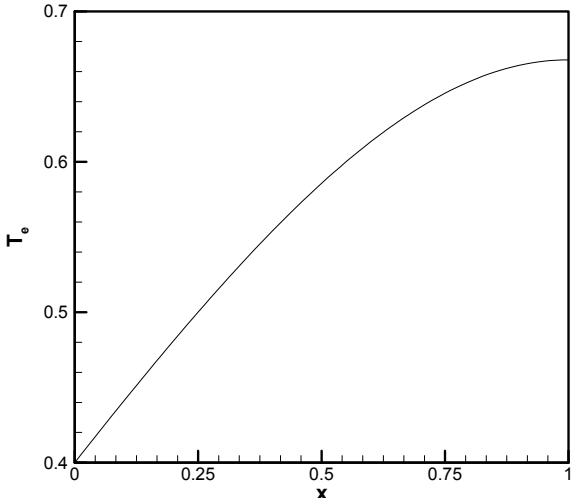

Figure 8. Normalized electron energy profile.

CONCLUSIONS

In this paper, a finite element based 1D formulation of plasma–sheath is given for a partially ionized plasma using the multi-component fluid equation. Based on the experimental data for multiple ionization of xenon gas, a third-order polynomial has been used in electron temperature as a fit to these processes. Such a polynomial has been used to self-consistently calculate the rate of ionization in the plasma continuity equations. For the neutral continuity equation a third order polynomial corresponding to 0+ and 0++ have been used.

It is seen that neutral density decreases in the bulk plasma region reaching a minima at the presheath-sheath boundary and then starts increasing in the sheath region. This can be attributed to the suppression of ionization in the near sheath region. The electron and neutral number density profiles near the sheath show their usual behavior. The ion number density keeps increasing in the bulk plasma and crosses the modified Bohm velocity near the presheath. The following questions remain to be answered. How does collisions inside the sheath affect the impact ion energy and consequently, sputtering yield? What role secondary emission and sputter yield plays in the sheath stability? Most intriguingly, how does magnetic field affects the sheath dynamics? We shall address some of these issues in our subsequent work.

ACKNOWLEDGEMENTS

This work was partially supported by the NASA research grant nos. NAG3-2520 and NAG3-2638 with D. Jacobson and D.R Reddy as technical monitors, respectively. The authors gratefully acknowledge many thoughtful discussions with NASA GRC electric propulsion group.

REFERENCES

[1]Morozov, A.I. and Savelyev, V. V., in *Reviews of Plasma Physics*, vol. 21, ed. B.B. Kadomtsev and V.D. Shafranov, Consultants Bureau, New York, , pp. 261, 2000.

[2]Shang, J. S., Hayes, J., Harris, S., Umstattd and Ganguly, B., AIAA 2000-2258, 31st AIAA Plasmadynamics and Lasers Conference, CO, 2000.

[3]Langmuir, I. And Tonk, L., Phys. Rev., Vol. 34, pp. 874, 1929.

[4]Valentini H.-B., Phys. Plasmas, Vol. 3, pp.1459, 1996.

[5]Valentini H.-B., Phys. Source Sci. Tech., Vol.9, pp.1574, 2000.

[6]Godyak, V. A. and Sternberg, N., Phys. Rev. A, Vol. 42, pp.2299, 1990.

[7]Sternberg N. and Godyak V. A., Physica D, Vol. 97, pp. 498,1996.

[8]Nitschke, T. E. and Graves, D. B., IEEE trans on Plasma Sci., Vol. 23, pp.717, 1995.

[9]Roy, S. and Baker, A.J., Numerical Heat Transfer – Part B, vol. 31, pp. 135, 1997.

[10]Roy, S. and Baker, A. J., Numerical Heat Transfer – Part B, Vol. 33, pp. 5, 1998.

[11]Mitchner, M. and Kruger, C. H., in *Partially ionized Gases*, Wiley-Interscience, New York, 1973.

[12]Pullins, S., Chiu, Y., Levandier, D. and Dressler, R., *38th Aerospace Sciences Meeting and Exhibit, Reno, NV, 2000* (AIAA, Washington DC, 2000), AIAA-2000-0603.

[13]Roy, S., Computer Methods in Applied Mechanics and Engineering, Vol. 184, pp. 87, 2000.

[14]Chen, F. F., *Introduction to Plasma Physics,* New York: Plenum, pp. 84, 1974